PHYSICAL REVIEW C VOLUME 41, NUMBER 3 MARCH 1990

Coupled reaction channels effects in the elastic scattering of $^{32,36}S+^{58,64}Ni$

A. M. Stefanini, A. Tivelli, G. Montagnoli, D. R. Napoli,* and D. Bonamini
Istituto Nazionale di Fisica Nucleare, Laboratori Nazionali di Legnaro, I-35020 Legnaro, Padova, Italy

S. Beghini, F. Scarlassara, and F. Soramel
Dipartimento di Fisica, Universitá di Padova and Istituto Nazionale di Fisica Nucleare, Sezione di Padova, Padova, Italy

C. Signorini
Dipartimento di Fisica, Universitá di Salerno and Istituto Nazionale di Fisica Nucleare, Sezione di Padova, Padova, Italy

A. DeRosa, G. Inglima, and M. Sandoli
Dipartimento di Fisica, Universitá di Napoli and Istituto Nazionale di Fisica Nucleare, Sezione di Napoli, Napoli, Italy

G. Cardella, M. Papa, and F. Rizzo
Dipartimento di Fisica, Universitá di Catania and Istituto Nazionale di Fisica Nucleare, Sezione di Catania, Catania, Italy
(Received 17 May 1989)

Elastic scattering angular distributions of $^{32,36}S$ (beams)$+^{58,64}Ni$ have been measured at several energies around the Coulomb barrier. An optical-model analysis of the data reveals remarkable energy dependences of the potentials at the strong absorption radii, in all cases. The largest effects are observed for $^{32}S+^{64}Ni$. This is due to the coupled reaction channels which also strongly influence the sub-barrier fusion cross sections. Coupled-channels calculations of elastic scattering and fusion have been performed, including the inelastic excitations of projectile and target; the need for considering additional (transfer) channels is made evident. We also have indications that sub-barrier fusion is not merely tunneling through a potential barrier, although energy dependent, as absorption into fusion takes place at larger internuclear distances. Older fusion and quasielastic transfer data are overviewed and compared with the reaction cross sections extracted from elastic scattering. Open questions still remain about the role of specific channels in determining the observed isotopic differences.

I. INTRODUCTION

The study of heavy-ion collisions around the Coulomb barrier offers the opportunity of observing spectacular effects due to the mechanisms of coupled reaction channels. The many facets of such processes were discussed in a recent symposium.[1] After the discovery of orders-of-magnitude cross section enhancements in the sub-barrier fusion (see Ref. 2 for a review), it was soon realized that a full understanding of those effects in terms of channel coupling[3] can only be accomplished when complete sets of data are available about the reaction channels competing with fusion in the same energy range. These channels are the quasielastic ones, i.e., inelastic excitations and transfer reactions of one or more nucleons or clusters. Only in a few cases[2] such studies were carried out so far, while a large body of data on sub-barrier fusion exists by now.

More recently, a complementary and equally interesting manifestation of the same phenomena, i.e., channel coupling, has been revealed[4,5] by analyses of elastic scattering measurements near the barrier. Here the evidence is a rather sharp energy dependence of the optical potential, which has been called "threshold anomaly." Its interpretation relies on the already known existence, on the basis of the causality principle, of a dispersion relation[6] connecting the real and imaginary parts of the potential. Near the barrier, where the absorption changes rapidly, one gets an additional attractive contribution to the real scattering potential, as the cooperative effect of many reaction channels. This enhanced attraction of the nuclear surfaces leads in turn to large sub-barrier fusion cross sections. The threshold anomaly has been so far observed in a few systems,[4,5,7,8] the case of $^{16}O+^{208}Pb$ (Ref. 4) being perhaps the clearest one. For that system there is also an early analysis of Delagrange *et al.*,[9] pointing to the same physical conclusion, i.e., that the real potential must be stronger at energies close to the barrier.

Moreover, it has been argued recently[10] that a description of the reaction mechanism within the optical model can be accomplished by the use of a short-ranged and sharp "fusion potential" confined within the Coulomb barrier, plus a surface absorption which simulates the quasielasic reaction channels. Other analyses,[11] however, point to the need for extending the range of the fusion potential allowing for absorption under and possibly outside the barrier. In Ref. 12, absorption into fusion at large internuclear distances has been attributed to the onset of neutron transfer which provides a driving force toward fusion; that model establishes a correlation between

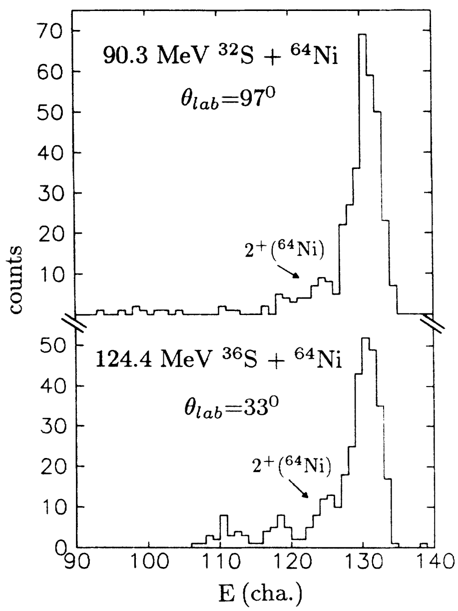

FIG. 1. Energy spectra of $A = 32$ particles (upper panel) and $A = 36$ particles (lower panel) from the reactions indicated.

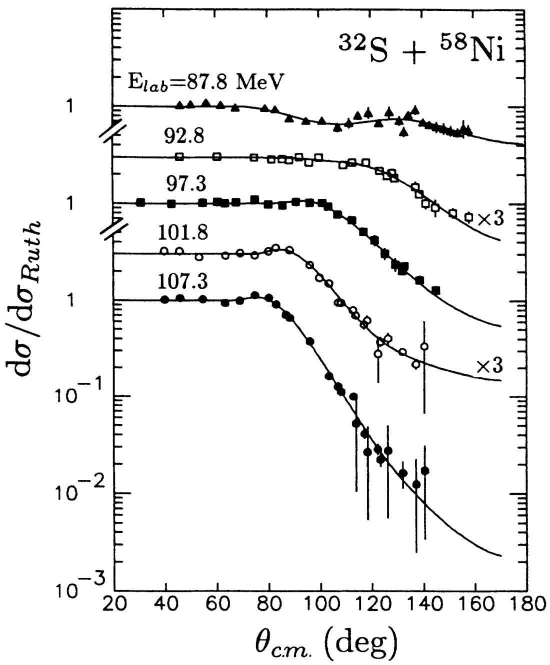

FIG. 3. Elastic scattering angular distributions for $^{32}S+^{58}Ni$ at various laboratory energies. The lines are optical-model fits performed with the code PTOLEMY.

neutron transfer and fusion and it has proved to be quite successful in various cases.

This paper presents the results of elastic scattering experiments in the four nearby systems $^{32,36}S+^{58,64}Ni$, showing evidence of strong energy dependences of the optical potential; a short account of the data with the ^{32}S beam has been given in a previous Letter.[8] Section II is a description of the experimental setup; Sec. III presents the experimental angular distributions and the corresponding optical-model fits trying to show to which extent a short-range fusion potential is adequate. The energy dependences of the fit potentials are discussed in Sec. IV, while Sec. V shows the results of coupled-channels calculations where the inelastic excitations of both projectile and target are included; in addition, the sub-

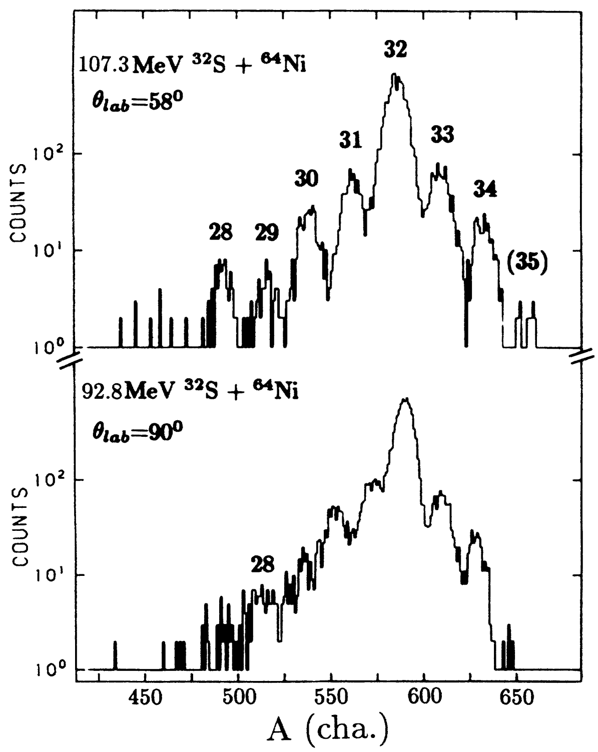

FIG. 2. Mass spectra of sulfur-like ions for the reactions indicated.

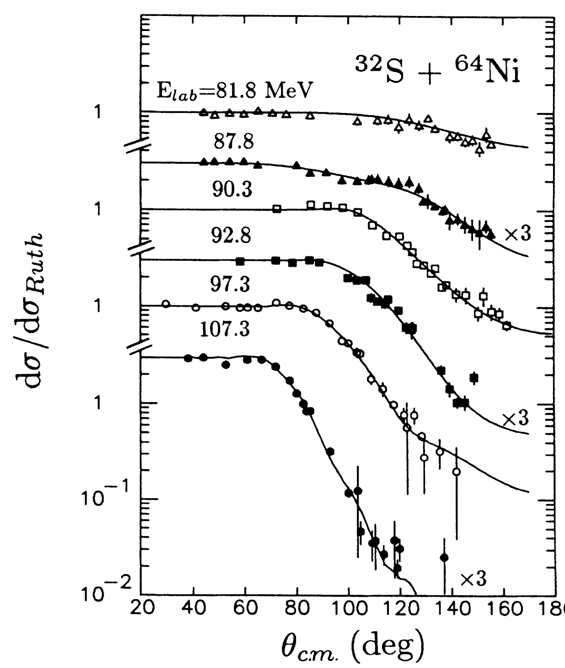

FIG. 4. Same as Fig. 3, but for $^{32}S+^{64}Ni$.

barrier fusion excitation functions are calculated in the same approach and compared with the corresponding data.[13] Section VI is a review of the quasielastic transfer cross sections,[14] together with the reaction cross sections extracted from the present scattering experiments. Section VII is a summary and concludes this paper.

II. EXPERIMENTAL

The present elastic scattering measurements were carried out at the Legnaro XTU Tandem accelerator which provided the ^{32}S and ^{36}S beams at several energies in the range 82–150 MeV. An FeS sample, enriched to around 40% in mass 36, was used in the sputtering ion source to produce the ^{36}S beam. Typical beam intensities were 10–50 particle nA. The Ni targets were placed in a 60 cm diameter sliding seal scattering chamber; they were 30 μg/cm^2 evaporations on 20 μg/cm^2 carbon foils, enriched to 99.8% and 96.5% in mass 58 and 64, respectively. The beam intensity and direction were monitored by two Si detectors placed at $\theta_{\rm lab}=\pm 16°$ and slightly below the reaction plane. They insured as well proper normalization of the measured elastic yields.

The scattered sulfur ions were detected by up to three time-of-flight–energy telescopes consisting of microchannel plates detectors and 200–300 mm^2 Si surface barrier detectors, the flight path being 80–100 cm. The telescopes were external to the scattering chamber; only one microchannel plates detector was lodged inside, at around 17 cm from the target, covering the backward angles. The limit was, anyway, $\theta_{\rm lab} \le 135°$. The uncertainty of the detection angle was estimated to be $\Delta\theta \simeq \pm 0.25°$, and an integration over $\pm 0.30°$–$0.40°$ occurred, depending on the Si detector used.

Mass and energy resolutions were $A/\Delta A \simeq 50$ and $\Delta E \simeq 700$–800 keV FWHM, which allowed a good separation of the elastic scattering from the quasielastic reaction channels. Only the lowest 2^+ excitation in the Ni targets gave some problems at the lowest energies and/or at the most backward angles; in those cases careful Gaussian fits of the energy spectra for $A=32$ (or $A=36$) were necessary. Figures 1 and 2 give two examples of energy and mass spectra in different experimental situations.

III. DATA AND OPTICAL-MODEL FITS

The elastic scattering angular distributions for the four systems at the various incident energies are shown in Figs. 3–6 and all data are listed in Tables I–IV. We recall here that the general systematics of Ref. 15 gives the following Coulomb barriers: $V_{b,\rm lab}=94.2$ (89.4) MeV for ^{32}S+$^{58(64)}$Ni and $V_{b,\rm lab}=96.6$ (91.6) MeV for ^{36}S+$^{58(64)}$Ni, respectively. The quoted errors in Figs. 3–6 are essentially the statistical uncertainties plus a (minor) contribution due to the corrections for the isotopical impurites in the targets. Those corrections were negligible in the case of ^{58}Ni and amounted typically to a few percent for ^{64}Ni. Possible systematic errors, coming, e.g., from a poor evaluation of solid angles, were corrected for by normalizing the elastic yields to the Rutherford limit at the most forward angles. We note that the angular distributions for the ^{36}S+Ni systems are at some energies not so rich of experimental points at those measured with the ^{32}S beam.

The optical-model code PTOLEMY (Ref. 16) was used to analyze the data, except those of 150 MeV ^{32}S+Ni (see Ref. 8). According to Ref. 10, the imaginary optical potential is explicitly divided[12] into two parts $W_D(r)$ and $W_F(r)$, so that the full nuclear potential is

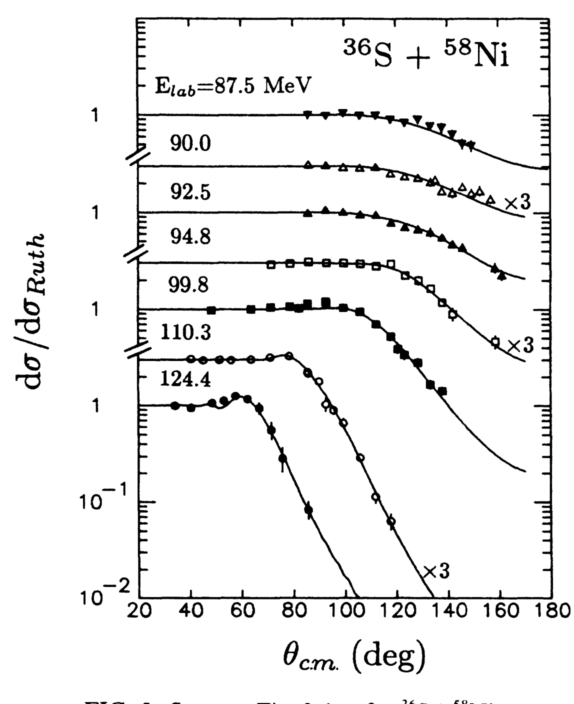

FIG. 5. Same as Fig. 3, but for ^{36}S+^{58}Ni.

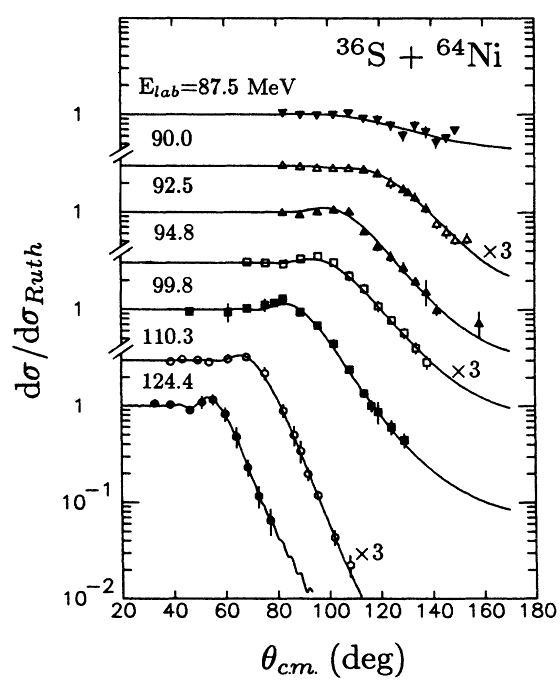

FIG. 6. Same as Fig. 3, but for ^{36}S+^{64}Ni.

$$U(r)=V(r)+i[W_F(r)+W_D(r)] ,$$

to which the Coulomb interaction has to be added. $W_D(r)$ takes care of the absorption into the quasielastic (direct) reaction channels and it is surface peaked:

$$W_D(r)=4W_Da_D\frac{d}{dr}\frac{1}{1+\exp(X_D)} ,$$

$$X_D=\frac{r-R_D}{a_D},\quad R_D=r_D(A_1^{1/3}+A_2^{1/3}) .$$

$W_F(r)$ and $V(r)$ have Woods-Saxon shapes. $W_F(r)$ is responsible for the absorption into fusion and it is chosen[10] to be a sharp potential confined within the barrier with depth $W_F=20$ MeV, radius parameter $r_F=1.0$ fm, and diffuseness $a_F=0.25$ fm in all cases. This assumption is equivalent to postulating that fusion takes place if, and only if, the Coulomb barrier has been tunneled or overcome.

An initial series of χ^2 searches were done, where four parameters of the full potential were varied, i.e., the real strength V and the three parameters of the surface interaction W_D, r_D, and a_D. The Coulomb radius parameter was always kept fixed to $r_c=1.20$ fm. The real diffuseness and the radius parameter were fixed to $a=0.5$ fm and $r_0=1.247$ (1.277) fm for $^{32(36)}$S, respectively, following the previous analysis[8] of ^{32}S+Ni. These four-parameter fits showed that r_D varies little with energy above the barrier (values between 1.40 and 1.50 fm were found), whereas a general trend is observed that r_D becomes larger at the lower energies for three of the four systems.

Then a second series of three-parameter fits were performed, by fixing r_D to the average values resulting from the above barrier energies, separately for each system. These searches yielded the real strengths V as well as W_D and a_D at every energy. The average values of r_D show an interesting systematics (see Table V): They scale almost perfectly with the number of neutrons and/or neutron holes outside the closed shells at $N=20$ and 28. The

TABLE I. Elastic scattering cross sections for ^{36}S+^{58}Ni.

E_{lab} (MeV)	$\theta_{c.m.}$ (deg)	$\frac{d\sigma_{el}}{d\sigma_{Ruth}}$	E_{lab} (MeV)	$\theta_{c.m.}$ (deg)	$\frac{d\sigma_{el}}{d\sigma_{Ruth}}$	E_{lab} (MeV)	$\theta_{c.m.}$ (deg)	$\frac{d\sigma_{el}}{d\sigma_{Ruth}}$
87.5	85.8	1.002±0.088		112.2	0.955±0.054		112.1	0.703±0.055
	92.7	0.979±0.060		118.0	0.793±0.062		117.9	0.521±0.044
	99.5	1.044±0.049		123.3	0.708±0.049		120.7	0.388±0.044
	105.8	0.987±0.064		128.4	0.673±0.058		123.2	0.336±0.035
	112.0	0.989±0.063		133.4	0.627±0.067		128.4	0.280±0.033
	117.8	0.899±0.069		137.9	0.557±0.037		133.4	0.167±0.018
	123.4	0.834±0.048		141.9	0.473±0.033		137.9	0.143±0.014
	128.5	0.899±0.084		145.9	0.434±0.043			
	133.4	0.769±0.062		158.6	0.270±0.031	110.3	40.4	1.018±0.066
	137.8	0.743±0.085		161.1	0.228±0.027		45.2	0.988±0.055
	142.0	0.636±0.066					51.5	0.999±0.055
	145.8	0.510±0.061	94.8	71.5	0.968±0.038		55.9	0.991±0.043
	149.3	0.487±0.064		78.8	0.988±0.066		63.6	1.004±0.043
				85.9	1.030±0.046		71.0	1.055±0.060
90.0	85.9	1.046±0.057		92.9	1.008±0.056		78.4	1.088±0.044
	92.7	1.032±0.054		99.6	1.006±0.067		85.5	0.745±0.049
	99.5	0.976±0.050		106.1	0.993±0.073		85.8	0.721±0.068
	105.8	0.969±0.070		112.2	0.936±0.044		90.0	0.597±0.054
	112.0	0.991±0.065		118.0	0.993±0.068		92.5	0.344±0.055
	117.9	0.855±0.068		123.5	0.751±0.050		95.5	0.299±0.030
	123.4	0.795±0.061		128.7	0.664±0.067		99.3	0.220±0.025
	128.5	0.767±0.057		133.5	0.550±0.050		105.8	0.097±0.010
	133.4	0.693±0.066		138.0	0.394±0.026		111.8	0.038±0.006
	135.2	0.731±0.070		142.1	0.299±0.044		117.7	0.021±0.004
	137.8	0.563±0.052		158.6	0.154±0.024			
	141.9	0.542±0.064				124.4	34.2	0.991±0.079
	145.8	0.622±0.059	99.8	48.3	0.983±0.061		40.3	0.943±0.060
	149.3	0.531±0.053		63.8	1.002±0.069		48.5	1.066±0.091
	152.6	0.564±0.062		71.3	1.047±0.070		53.0	1.121±0.105
	156.8	0.466±0.048		78.7	1.064±0.064		57.6	1.259±0.098
				82.3	1.022±0.067		62.2	1.164±0.102
92.5	85.7	0.993±0.045		85.6	1.144±0.057		66.8	0.939±0.128
	92.6	1.073±0.055		92.6	1.208±0.062		71.4	0.561±0.114
	99.5	1.018±0.062		99.5	1.036±0.063		75.7	0.286±0.081
	106.1	0.960±0.053		105.9	0.947±0.062		85.7	0.083±0.017

smallest r_D is in fact found for $^{36}S+^{58}Ni$ and the largest one for $^{32}S+^{64}Ni$.

A third series of fits was finally performed for those cases where the surface radius had the tendency to be significantly larger (or smaller) than the average values, retaining the real strengths (already determined) and varying again W_D, r_D, and a_D. Only a few exceptions to these general rules had to be done, when the quality of the fits was found to be really unacceptable. But otherwise, the spirit of this analysis was to extract general trends of the potentials with a reasonably small number of free parameters; the price we paid for this is to have some cases where the χ^2 values are not particularly good.

The final fits are shown in Figs. 3–6 as full lines and the corresponding potential parameters are listed in Table V together with the deduced reaction cross sections and the χ^2 values. For $^{32}S+Ni$ scattering at the lowest energies a broad structure appears in the backward angular distributions, which was already noticed[8] and whose nature is still unclear. In these cases the extracted reaction cross sections are rather large, and they are shown within parentheses in Table V.

Apart from this, the chosen potential parametrization (with a sharp fusion potential confined within the barrier) seems to give a good account of the experimental angular distributions. However, there are a few cases where the surface absorption turns out to be very deep and sharp, e.g., the scattering of $^{32}S+^{58}Ni$ at 101.8 MeV where $W_D=4.57$ MeV and $a_D=0.12$ fm. This leads to imaginary potentials of unusual shapes, casting some doubts about their physical significance. It then appears that one should relax the assumption about the fusion potential and let the corresponding absorption extend at larger radii. This kind of approach has been successfully followed by Udagawa[17] for the scattering of $^{32}S+Ni$, in the spirit of their work[11] on $^{16}O+^{208}Pb$ where they claim that there is no way to avoid making the fusion radius as large as 1.40 fm. In a very recent analysis[18] of the scattering of 88 MeV $^{32}S+^{64}Ni$, the fusion potential is assumed to have a surface portion in addition to the more internal volume absorption; the approach seems successful and predicts moreover wider spin distributions of the com-

TABLE II. Elastic scattering cross sections for $^{36}S+^{64}Ni$.

E_{lab} (MeV)	$\theta_{c.m.}$ (deg)	$d\sigma_{el}/d\sigma_{Ruth}$	E_{lab} (MeV)	$\theta_{c.m.}$ (deg)	$d\sigma_{el}/d\sigma_{Ruth}$	E_{lab} (MeV)	$\theta_{c.m.}$ (deg)	$d\sigma_{el}/d\sigma_{Ruth}$
87.5	82.6	1.030±0.071		96.0	1.029±0.065		102.1	0.447±0.047
	89.3	0.981±0.072		102.3	1.083±0.062		108.1	0.242±0.021
	95.8	0.974±0.073		108.3	1.031±0.068		113.7	0.136±0.014
	102.0	0.989±0.062		114.0	0.640±0.054		116.5	0.101±0.013
	108.0	1.027±0.060		119.2	0.449±0.048		119.1	0.087±0.022
	113.8	0.899±0.066		124.3	0.352±0.039		124.2	0.061±0.010
	119.3	0.881±0.093		129.3	0.273±0.034		129.3	0.045±0.007
	124.4	0.771±0.085		133.9	0.198±0.018			
	129.2	0.608±0.071		138.0	0.155±0.046	110.3	39.1	0.969±0.080
	133.7	0.763±0.082		142.1	0.100±0.013		43.5	1.030±0.068
	138.0	0.666±0.085		158.5	0.073±0.022		49.5	1.008±0.077
	142.0	0.517±0.061					53.9	0.961±0.075
	145.8	0.573±0.052	94.8	68.9	1.018±0.054		61.3	1.032±0.100
	149.3	0.688±0.056		75.9	1.002±0.074		68.3	1.080±0.057
				82.8	0.980±0.063		75.5	0.736±0.112
90.0	82.6	1.029±0.064		89.5	1.105±0.083		82.5	0.298±0.046
	89.3	1.000±0.078		96.0	1.180±0.072		86.7	0.167±0.038
	95.9	0.963±0.051		102.3	1.023±0.066		89.1	0.115±0.029
	102.0	0.963±0.052		108.3	0.744±0.082		91.9	0.066±0.010
	108.0	0.954±0.063		113.9	0.549±0.060		95.7	0.040±0.004
	113.8	0.929±0.086		119.4	0.362±0.045		102.0	0.015±0.003
	119.3	0.853±0.077		124.5	0.261±0.023		107.8	0.0075±0.002
	124.3	0.688±0.065		129.4	0.192±0.023			
	129.2	0.591±0.054		138.2	0.096±0.014	124.4	32.9	1.064±0.082
	131.1	0.544±0.037		133.9	0.134±0.018		38.9	1.032±0.090
	133.7	0.482±0.049					46.5	0.904±0.080
	138.0	0.372±0.041	99.8	46.5	0.955±0.066		51.1	1.100±0.160
	142.0	0.257±0.030		61.4	0.936±0.194		55.4	1.167±0.143
	145.8	0.210±0.030		68.7	1.023±0.056		60.0	0.823±0.132
	149.3	0.176±0.019		75.7	1.115±0.160		64.4	0.481±0.113
	153.8	0.179±0.021		79.2	1.169±0.041		68.7	0.232±0.045
				82.5	1.297±0.099		72.8	0.117±0.030
92.5	82.6	1.013±0.053		89.1	0.948±0.050		77.1	0.066±0.020
	89.3	0.958±0.053		95.9	0.687±0.031			

pound nucleus, which would be interesting to compare with experimental data so far not available, unfortunately.

A further check on the validity of the potentials of Table V may come from the fusion (absorption) cross sections which they yield in comparison with the corresponding experimental values. We shall come back to this in Sec. VII; now we keep our analysis scheme and discuss the energy dependence of the potentials in the vicinity of the strong absorption radii, where they are most unambiguously determined.

IV. THRESHOLD ANOMALIES

The analysis of the preceding section has yielded us the potentials of Table V; their real and imaginary parts were evaluated at $r(\theta_{1/4})$ (quarter point) and plotted in Figs. 7 and 8 vs the bombarding energy. In order to have an estimate of the accuracy of those values, error bars have been drawn for the real potentials, which correspond to a 10% increase of the χ^2 values of the fits obtained by fixing the surface absorption parameters; according to the same criterion, by varying only W_D we could assign uncertainties to the imaginary potentials. Error bars smaller than the symbols are not shown.

The lowest energies, where the scattering data do not show any quarter point in the angular distribution, correspond to situations where the nuclei do not come close enough to each other to allow an unambiguous determination of the potentials. As a consequence, the error bars for the corresponding points in Fig. 7 are very large,

TABLE III. Elastic scattering cross sections for $^{32}S+{}^{58}Ni$.

E_{lab} (MeV)	$\theta_{c.m}$ (deg)	$\frac{d\sigma_{el}}{d\sigma_{Ruth}}$	E_{lab} (MeV)	$\theta_{c.m.}$ (deg)	$\frac{d\sigma_{el}}{d\sigma_{Ruth}}$	E_{lab} (MeV)	$\theta_{c.m}$ (deg)	$\frac{d\sigma_{el}}{d\sigma_{Ruth}}$
87.8	46.2	1.043±0.049		126.3	0.646±0.051		88.4	1.104±0.028
	50.4	1.053±0.041		128.2	0.693±0.069		96.2	0.776±0.018
	56.4	1.101±0.041		129.2	0.613±0.038		99.9	0.574±0.050
	62.0	1.040±0.041		137.2	0.497±0.063		103.5	0.504±0.018
	67.6	0.973±0.037		138.7	0.420±0.038		107.0	0.320±0.026
	79.1	0.964±0.041		141.2	0.336±0.041		108.2	0.317±0.017
	83.0	0.933±0.038		144.9	0.306±0.061		112.8	0.265±0.019
	88.6	0.756±0.041		151.8	0.269±0.032		113.8	0.233±0.017
	95.0	0.714±0.035		158.0	0.245±0.033		117.0	0.188±0.021
	101.2	0.717±0.062					118.2	0.207±0.025
	107.2	0.611±0.061	97.3	30.9	1.024±0.067		122.3	0.093±0.046
	111.6	0.678±0.081		42.7	0.991±0.057		123.3	0.124±0.014
	115.1	0.804±0.076		54.8	1.015±0.061		126.3	0.135±0.019
	119.2	0.862±0.109		60.5	1.040±0.056		131.9	0.098±0.007
	123.3	0.677±0.057		63.4	1.010±0.060		137.1	0.073±0.008
	127.3	0.878±0.111		67.7	1.035±0.060		140.4	0.112±0.090
	131.1	0.713±0.079		75.0	1.105±0.037			
	132.9	0.552±0.061		80.2	0.983±0.046	107.3	40.0	1.021±0.056
	134.6	0.820±0.062		85.6	0.960±0.029		45.9	1.062±0.057
	137.3	0.922±0.097		90.9	1.043±0.056		54.7	1.036±0.051
	140.3	0.690±0.051		96.2	1.027±0.027		63.3	0.942±0.048
	142.7	0.649±0.056		101.1	1.018±0.036		69.1	0.999±0.040
	145.6	0.620±0.076		103.4	0.938±0.047		74.9	1.141±0.056
	148.4	0.595±0.077		107.0	0.776±0.060		80.3	1.069±0.056
	151.1	0.563±0.061		112.5	0.671±0.056		83.2	0.916±0.033
	153.8	0.543±0.052		117.0	0.509±0.044		86.9	0.709±0.032
	156.2	0.602±0.126		121.2	0.417±0.051		88.4	0.660±0.023
	158.0	0.576±0.069		125.3	0.304±0.040		96.1	0.376±0.015
				129.3	0.236±0.035		103.4	0.164±0.011
92.8	46.1	1.010±0.040		132.0	0.203±0.018		107.0	0.127±0.013
	60.5	1.011±0.053		132.8	0.227±0.021		108.1	0.112±0.006
	74.8	0.993±0.035		138.7	0.163±0.016		112.9	0.100±0.008
	81.6	0.952±0.025		145.0	0.129±0.013		113.9	0.053±0.042
	85.7	0.960±0.041					117.1	0.041±0.005
	88.5	0.932±0.067	101.8	39.8	1.071±0.069		118.3	0.027±0.021
	92.2	1.005±0.063		45.8	1.070±0.050		122.2	0.029±0.004
	96.1	0.888±0.056		53.3	0.924±0.042		123.3	0.022±0.003
	99.9	1.001±0.044		63.5	0.962±0.036		126.2	0.028±0.022
	109.3	0.837±0.076		69.2	1.024±0.061		131.9	0.016±0.005
	112.8	0.886±0.074		74.8	0.973±0.036		137.2	0.013±0.010
	118.2	0.882±0.045		80.2	1.073±0.046		140.4	0.017±0.014
	123.5	0.728±0.056		83.1	1.164±0.032			

and the lowest energy point for $^{36}S+^{58}Ni$ has been left out of Fig. 8.

Strong variations with energy are observed in all cases. As the energy decreases and reaches the barrier region, the absorption is more and more reduced. At the same time, the real potential increases and shows a broad maximum around the barrier position. The results for $^{32}S+Ni$ are in good agreement with those obtained previously.[8]

The lines in Figs. 7 and 8 are the calculated dispersive corrections for the various systems, making use of the dispersion relation in its subtracted form[6] and of a simple linear model for W rising from zero to W_0 (in absolute value) in the interval (E_a, E_b) and then remaining con-

TABLE IV. Elastic scattering cross sections for $^{32}S+^{64}Ni$.

E_{lab} (MeV)	$\theta_{c.m.}$ (deg)	$d\sigma_{el}/d\sigma_{Ruth}$	E_{lab} (MeV)	$\theta_{c.m.}$ (deg)	$d\sigma_{el}/d\sigma_{Ruth}$	E_{lab} (MeV)	$\theta_{c.m.}$ (deg)	$d\sigma_{el}/d\sigma_{Ruth}$
81.8	44.5	1.007±0.032		151.2	0.201±0.067	97.3	29.8	1.048±0.079
	48.8	0.946±0.040		153.8	0.232±0.034		41.5	0.965±0.064
	54.4	0.988±0.044		155.7	0.194±0.025		53.0	1.004±0.049
	60.0	0.972±0.045					58.5	0.971±0.073
	65.4	1.047±0.035	90.3	72.8	1.025±0.068		61.4	0.974±0.044
	71.0	0.996±0.038		85.9	1.139±0.092		65.4	0.969±0.068
	76.4	0.967±0.042		92.3	1.100±0.044		72.5	1.095±0.028
	85.5	0.939±0.071		98.2	1.064±0.044		77.6	1.022±0.050
	103.7	0.822±0.078		104.1	0.960±0.041		83.0	0.954±0.023
	111.6	0.837±0.083		109.7	0.702±0.030		87.9	0.869±0.041
	115.8	0.855±0.096		115.1	0.551±0.051		93.1	0.676±0.019
	119.8	0.722±0.105		120.2	0.545±0.020		97.9	0.442±0.021
	123.8	0.862±0.121		123.2	0.436±0.020		100.3	0.420±0.017
	127.6	0.748±0.086		125.1	0.375±0.030		103.6	0.336±0.039
	131.3	0.890±0.060		127.0	0.283±0.026		104.9	0.329±0.020
	133.8	0.693±0.036		129.7	0.273±0.021		109.1	0.179±0.023
	139.5	0.571±0.077		132.4	0.224±0.014		113.6	0.141±0.023
	142.6	0.579±0.060		134.1	0.254±0.022		117.8	0.098±0.009
	145.5	0.504±0.055		136.6	0.161±0.014		121.8	0.077±0.014
	148.4	0.525±0.063		138.2	0.170±0.015		122.9	0.057±0.046
	151.2	0.429±0.072		142.1	0.136±0.022		125.7	0.076±0.015
	153.8	0.607±0.104		145.9	0.135±0.025		128.5	0.047±0.005
	155.7	0.484±0.034		150.7	0.087±0.015		129.4	0.028±0.016
87.8	44.6	1.033±0.041		152.7	0.132±0.029		135.5	0.032±0.011
	48.7	1.050±0.049		155.9	0.090±0.017		141.9	0.020±0.016
	54.5	1.050±0.040		158.9	0.086±0.014	107.3	38.5	0.978±0.061
	60.0	1.046±0.044		161.8	0.065±0.008		44.4	1.003±0.057
	65.4	0.962±0.036					53.0	0.842±0.077
	80.3	0.954±0.038	92.8	58.6	0.972±0.042		61.2	0.952±0.046
	85.6	0.802±0.040		72.4	1.000±0.052		66.8	0.953±0.034
	91.8	0.814±0.039		78.8	0.951±0.060		72.2	0.806±0.028
	97.9	0.677±0.066		85.4	1.010±0.055		77.7	0.579±0.031
	103.8	0.670±0.039		89.2	0.961±0.058		80.4	0.426±0.024
	108.3	0.683±0.072		100.2	0.665±0.046		82.9	0.333±0.031
	109.4	0.698±0.068		103.7	0.628±0.050		84.1	0.280±0.018
	111.7	0.698±0.073		107.2	0.632±0.041		85.4	0.281±0.015
	115.9	0.659±0.080		109.2	0.416±0.045		93.1	0.108±0.010
	119.8	0.635±0.071		111.6	0.382±0.029		100.1	0.040±0.004
	123.8	0.653±0.084		114.7	0.356±0.033		103.6	0.042±0.033
	127.7	0.562±0.064		115.7	0.402±0.018		104.8	0.016±0.004
	129.4	0.417±0.037		119.7	0.309±0.020		109.2	0.012±0.004
	131.2	0.420±0.070		122.8	0.204±0.026		110.4	0.012±0.006
	133.8	0.371±0.021		124.8	0.194±0.039		113.7	0.009±0.002
	137.1	0.333±0.033		125.3	0.203±0.028		117.8	0.013±0.008
	137.9	0.346±0.032		136.3	0.074±0.008		118.8	0.007±0.001
	139.6	0.268±0.056		139.5	0.047±0.008		119.8	0.010±0.003
	142.7	0.274±0.036		142.5	0.034±0.004		137.1	0.008±0.005
	145.5	0.243±0.046		145.4	0.035±0.006			
	148.4	0.219±0.051		149.1	0.063±0.010			

stant. The corresponding algebraic expression for the real polarization potential is

$$\Delta V(E)=\frac{W_0}{\pi}(\epsilon_a \ln|\epsilon_a|-\epsilon_b \ln|\epsilon_b|) ,$$

where

$$\epsilon_i=\frac{E-E_i}{\Delta_0}, \quad i=a,b, \quad \Delta_0=E_b-E_a .$$

The adopted values in MeV for W_0, E_a, and E_b are 1.80 (0.92), 83.2 (87.8), and 92.8 (99.4) for $^{32}S+^{64(58)}Ni$, and 0.82 (0.44), 87.5 (87.5), and 102.5 (99.8) for $^{36}S+^{64(58)}Ni$, respectively. They resulted from a simple fit of the "experimental" imaginary potentials. The calculated ΔV are normalized to the data at the highest energies shown in the figures, for each system.

The fitting potentials satisfy only qualitatively the dispersion relation. This is especially true for $^{32}S+^{64}Ni$ where the calculated real polarization potential is much stronger than indicated by the data; in the cases of $^{36}S+Ni$ the smooth increase of the absorption with energy (smoother than with ^{32}S) leads to rather gentle variations of the real potentials around the barrier, whereas the data indicate sharper variations. All this can probably be expected due to the schematicity of the model for W and to the large degree of uncertainty in the choice of the parameters W_0, E_a, and E_b; unavoidable ambiguities in the elastic scattering fits have to be taken into account too. Anyway, the positions of the maxima in the real potentials are well reproduced.

A difference exists between $^{32}S+^{64}Ni$ and the other three cases: in that system there is much more absorption at all energies and the threshold anomaly is more remarkable, as the real potential increases by a factor larger than 3, when going from above to around the barrier. In the other systems those factors are all in the range $\simeq 1.6-2.0$.

Actually, $^{32}S+^{64}Ni$ displays the largest enhancement of sub-barrier fusion cross sections[13] which in a reduced scale exceed by about one order of magnitude those of the other systems. In other words, the cooperative effect of the many quasielastic reaction channels, which produces the strongest polarization potential in $^{32}S+^{64}Ni$, enhances considerably the sub-barrier fusion as well.

V. COUPLED-CHANNELS CALCULATIONS

We have used the results of the fits described in Sec. III in coupled-channels (CC) calculations of both elastic scattering and fusion, by substituting the surface absorption by explicit reaction channels and using again the code PTOLEMY. The lowest 2^+ and 3^- excitations of both projectile and target were included in the coupling scheme and the coupling strengths were derived from the experimental $B(E2)$ and $B(E3)$ data, as, e.g., in Ref. 3.

TABLE V. Optical-model parameters resulting from the fits to the elastic scattering data. Fixed parameters are underlined. In addition, the real diffuseness and radius parameter were fixed to $a=0.5$ fm and $r_0=1.247$ (1.277) fm for $^{32(36)}S$, respectively. The fusion potential was $W_F=20$ MeV, $a_F=0.25$ fm, and $r_F=1.0$ fm (see text). For 87.8 MeV $^{32}S+^{58}Ni$ the real diffuseness was fixed to 0.6 fm.

System	E_{lab} (MeV)	V (MeV)	W_D (MeV)	a_D (fm)	r_D (fm)	χ^2	σ_r (mb)
$^{36}S+^{64}Ni$	87.5	62.41	0.40	0.140	1.689	1.49	1.47
	90.0	69.26	0.38	0.585	<u>1.474</u>	0.31	221
	92.5	88.08	2.09	0.202	<u>1.474</u>	0.82	266
	94.8	70.28	4.50	0.237	<u>1.430</u>	0.52	315
	99.8	55.45	2.66	0.203	<u>1.474</u>	0.72	500
	110.3	48.23	2.24	0.320	<u>1.474</u>	0.11	920
	124.4	42.77	2.98	0.221	<u>1.474</u>	0.13	1183
$^{36}S+^{58}Ni$	87.5	58.80	1.26	0.198	1.669	0.55	(146)
	90.0	41.61	0.56	0.152	1.694	0.47	138
	92.5	59.92	0.44	0.305	1.614	0.50	170
	94.8	58.84	0.75	0.514	<u>1.419</u>	0.40	166
	99.8	43.72	1.87	<u>0.350</u>	<u>1.419</u>	1.75	286
	110.3	39.54	2.73	0.340	<u>1.419</u>	0.38	632
	124..4	42.45	3.83	0.237	1.423	0.48	924
$^{32}S+^{64}Ni$	81.8	85.90	1.25	0.554	<u>1.503</u>	1.01	178
	87.8	78.76	0.36	1.034	1.517	0.85	(506)
	90.3	83.31	3.27	0.204	<u>1.503</u>	1.91	283
	92.8	36.84	3.26	0.264	<u>1.503</u>	2.66	415
	97.3	34.62	4.30	0.243	<u>1.503</u>	1.08	581
	107.3	28.56	4.14	0.330	1.469	1.20	928
$^{32}S+^{58}Ni$	87.8	81.21	0.23	0.418	1.914	1.43	(396)
	92.8	74.05	0.50	0.659	<u>1.440</u>	0.75	215
	97.3	77.42	4.43	0.234	<u>1.440</u>	0.98	279
	101.8	72.11	4.57	0.120	1.483	1.05	406
	107.3	44.93	3.43	0.271	<u>1.440</u>	1.26	583

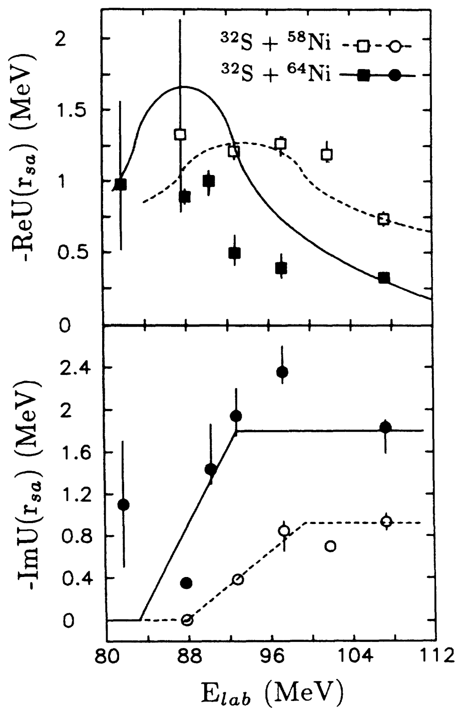

FIG. 7. The optical potential of $^{32}S+^{58,64}Ni$ vs the incident energy. The adopted strong absorption radii [identified with $r(\theta_{1/4})$] are $r_{sa}=11.18$ (10.83) fm for $^{32}S+^{64(58)}Ni$. By assuming for $W(E)$ the schematic behavior (lower panel) shown by full and dashed lines for the two systems, the real potential curves shown in the upper panel result from the dispersion relation.

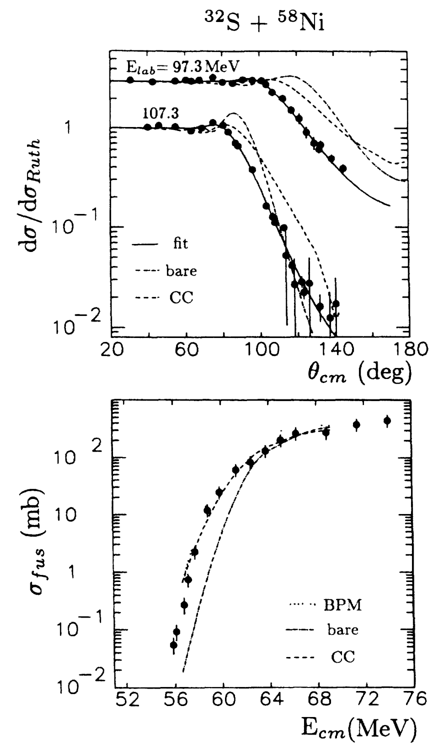

FIG. 9. Elastic scattering angular distributions at two representative energies (upper panel) and fusion excitation functions (lower panel) for $^{32}S+^{58}Ni$ (see text).

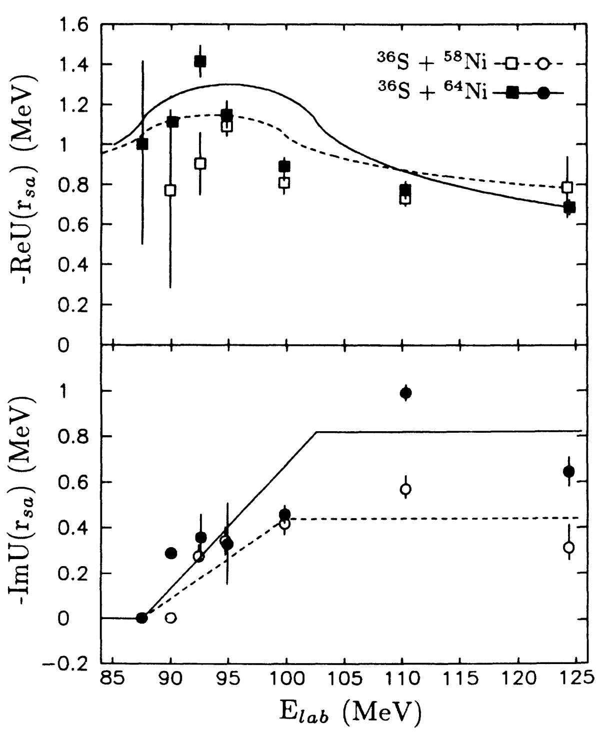

FIG. 8. Same as Fig. 7, but for $^{36}S+^{58,64}Ni$. The strong absorption radii are $r_{sa}=11.38$ (11.14) fm for $^{36}S+^{64(58)}Ni$.

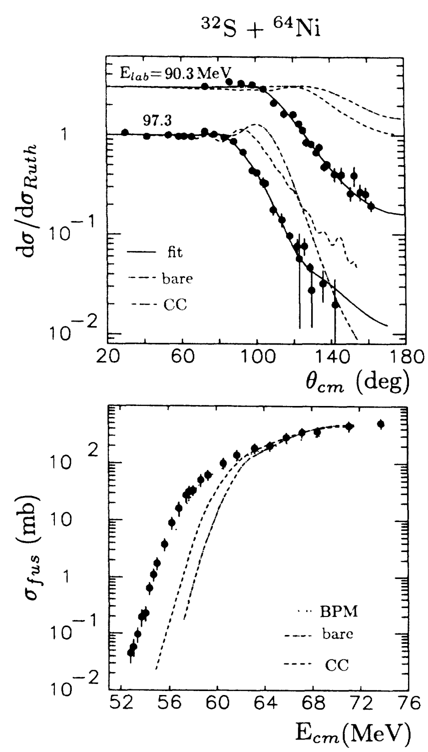

FIG. 10. Same as Fig. 9, but for $^{32}S+^{64}Ni$.

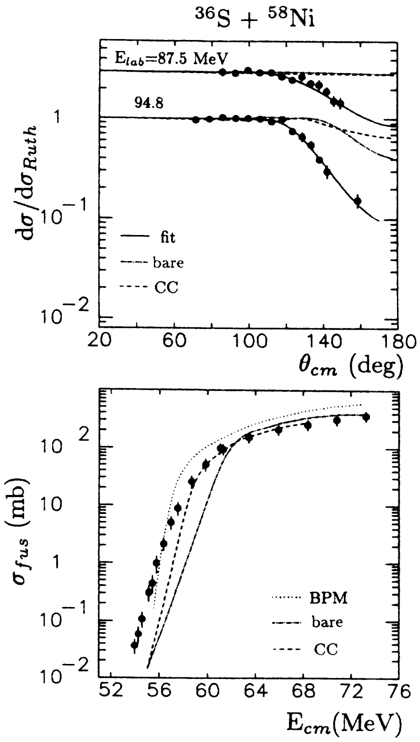

FIG. 11. Same as Fig. 9, but for $^{36}S+^{58}Ni$.

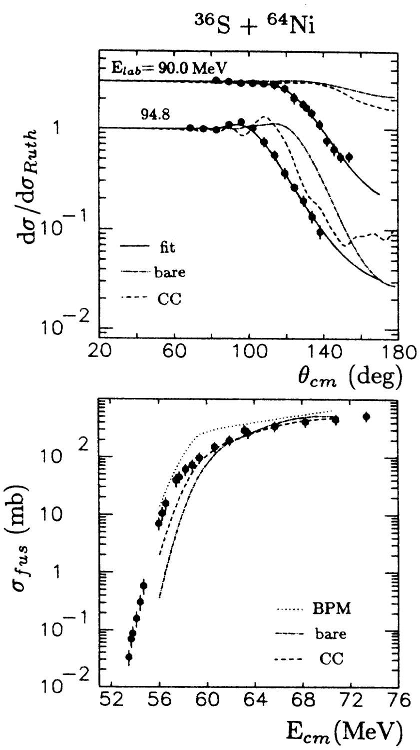

FIG. 12. Same as Fig. 9, but for $^{36}S+^{64}Ni$.

The "bare" potential was chosen according to the following prescriptions: (i) The geometry of the real part was that used in the elastic scattering fits; (ii) its strength was near to the fitting value at $E_{lab}=107.3$ (110.3) MeV for $^{32(36)}S$ (i.e., beyond the main part of the threshold anomaly), with a renormalization determined by the further constraint that the experimental fusion cross section is correctly calculated at those energies, separately for each system; this has led to shallower real potentials in all cases but $^{32}S+^{64}Ni$; (iii) the volume absorption was the same as described in Sec. III; (iv) no surface potential was introduced.

Representative results for the four systems (two energies each) are shown in the upper panels of Figs. 9–12 (dashed lines) in comparison with the experimental data. In addition, the angular distributions calculated with the bare potential without any coupling (dashed-dotted lines) are shown for reference as well as the fits (potentials of Table V, full lines). The CC calculations strongly overestimate the elastic scattering cross sections and consequently underpredict the reaction cross sections; this is a systematic feature which shows up at all energies for each system, and which points to the need for coupling additional channels. Since the effect of coupling higher lying inelastic states has been checked to be a minor contribution, we have evidence for the importance of transfer channels in determining the scattering cross sections. In fact we know from previous measurements that quasielas-

TABLE VI. Optical potentials for $^{32}S+^{64}Ni$ at $E_{lab}=107.3$ MeV. The volume absorption is as in Table V; fixed parameters are underlined. The fusion cross sections are calculated at $E_{lab}=92.8$ MeV where the experimental value is $\sigma_{fus}=26\pm6$ mb. Case 1 is the adopted potential of Table V, while in cases 1-a and 1-b the same parameters were used but the strengths of the coupled channels were varied (see text).

Potential	V (MeV)	a (fm)	r_0 (fm)	W_D (MeV)	a_D (fm)	r_D (fm)	χ^2	σ_{fus}^{CC} (mb)
1	44.93	0.500	1.247	3.43	0.271	1.440	1.26	16.8
1-a								20.1
1-b								13.5
A	50.00	0.407	1.301	3.20	0.264	1.440	1.19	55.6
B	44.52	0.445	1.281	3.30	0.272	1.440	1.25	41.7
C	100.00	0.260	1.366	1.83	0.279	1.440	1.16	80.5
D	182.54	0.60	1.069	3.60	0.267	1.440	1.45	11.3
E	346.75	0.395	1.20	3.15	0.264	1.440	1.19	62.7

TABLE VII. Transfer, inelastic, fusion, and total reaction cross sections. The center of mass Coulomb barriers (Ref. 15) are 60.7 and 59.6 MeV for $^{32}S+^{58,64}Ni$, and 59.6 and 58.6 MeV for $^{36}S+^{58,64}Ni$, respectively.

System	E_{lab} (MeV)	$E_{c.m.}$ (MeV)	σ_{tr} (mb)	σ_{in} (mb)	σ_{fus} (mb)	σ_{sum} (mb)	σ_r (mb)
$^{32}S+^{58}Ni$	107.3	69.1	65±7	273	294±59	632	583
	101.8	65.6	(50)	227	236±47	(513)	406
	97.3	62.7	34±6	186	94±21	314	279
	92.8	59.8	9±5	153	26±6	188	215
$^{32}S+^{64}Ni$	107.3	71.5	223±10	319	465±92	1007	928
	97.3	64.7	159±18	236	228±41	623	581
	92.8	61.9	121±12	194	145±29	460	415
	90.3	60.2	94±7	171	91±18	356	283
	81.8	54.5	23±6	118	0.9±0.2	142	178
$^{36}S+^{58}Ni$	110.3	68.0	127±27	250	256±52	633	632
	99.8	61.6	106±25	144	109±24	359	286
	94.8	58.5	48±10	105	23.1±6.5	176	166
$^{36}S+^{64}Ni$	110.3	70.6	80±18	272	453±91	805	920
	99.8	63.9	36±9	192	293±59	521	500
	94.8	60.7	32±7	150	150±30	315	306

tic transfer contributes significantly to the total reaction cross section in this range of energies, although the isotopic differences are relevant (see also Sec. VI).

The lower panels of Figs. 9–12 show the experimental fusion excitation functions together with the (smoothed) CC results; the no-coupling limit (i.e., absorption by the bare potential) is also reported. The calculations have been limited to the energy range where elastic scattering was measured. The CC results are in good agreement with the data only for $^{32}S+^{58}Ni$; otherwise, they underestimate the $^{36}S+^{58,64}Ni$ cross sections and the largest discrepancy is seen for $^{32}S+^{64}Ni$, where transfer seems therefore to play a particularly significant role.

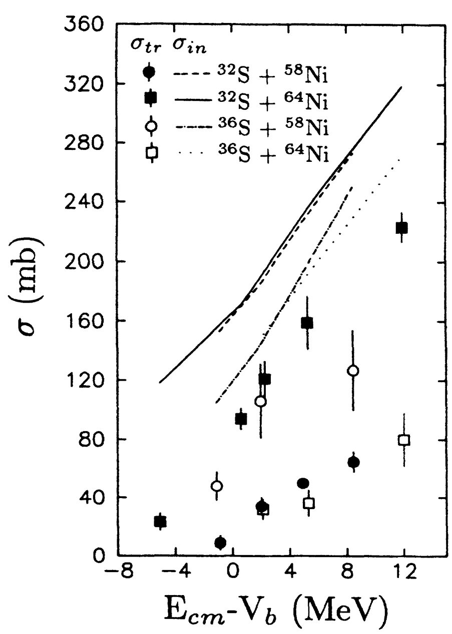

FIG. 13. Inelastic and total transfer cross sections versus the energy distance from the barrier (Ref. 15) for the four investigated systems.

The predictions of the energy-dependent barrier penetration model (BPM) appear in Figs. 9–12 too (dotted lines). The procedure to obtain them is the following: at each energy where elastic scattering was measured and fitted as described in Sec. III the reaction cross section was calculated using the Woods-Saxon part of the fitting potential (i.e., no surface absorption was included). That reaction cross section is the BPM fusion cross section by definition.[10] It is known[19,20] that a simple renormalization of the real potential strength at the various energies, as in this work, produces incorrect spin distributions of the compound nucleus; however, data on such spin distributions for the S+Ni systems are not available, as remarked in Sec. III.

The BPM cross sections allow similar comments as already done for the CC calculations of fusion. They are systematically larger than the CC results and, except for some overestimation at high energies, the overall agreement with the data is fair in all cases; this is true also for $^{32}S+^{64}Ni$, whose sub-barrier cross sections are badly underpredicted by the CC calculations which only include inelastic channels. One may argue that transfer channels produce a significant part of the real potential renormalization in that system, keeping in mind, however, the twofold uncertainties existing in the BPM and CC calculations of fusions: the results are model dependent, not only because of the choice of the fusion potential $W_F(r)$ which *a priori* models the fusion process, but also in view of the large ambiguities in determining the optical potential from elastic scattering at internuclear distances shorter than the strong absorption radius (i.e., the Coulomb barrier is largely fit dependent); the worst situations are found at the lowest energies, where the elastic scattering has no quarter point. In addition, for CC calculations one has to allow for the uncertainties in the measured values of the $B(E\lambda)$ strengths.

All such ambiguities were checked to some extent in a representative case ($^{32}S+^{58}Ni$) where transfer is manifestly playing a negligible role, by performing further CC calculations where (i) the strengths of the coupled inelastic excitations were all put to the extremes ($\pm 10\%$ typically) allowed by the errors in their adopted values (cases 1-a and 1-b in Table VI) but with no change in the potential parameters, or (ii) the adopted values of the strengths were kept, but five additional potentials (also listed in Table VI) were used: all of them yield good and almost indistinguishable fits to the elastic scattering data at 107.3 MeV and their real parts (used as bare potentials) span a wide range of strengths, radii, and/or diffusenesses.

The resulting fusion cross sections for $E_{\rm lab} = 92.8$ MeV (i.e., near to the top of the barrier) are shown in Table VI and large differences show up: Varying the inelastic strengths is apparently less dramatic than changing the potential and an overall uncertainty of a factor 10 is clear. Allowing also for changes in the fusion potential (volume absorption) would certainly enhance the ambiguity. In view of all this and as a conclusion of this section, we can say that the fair agreement between calculations and fusion data for three of the four systems is not a strong indication that the fitting potentials of Table V rely on sound physical assumptions.

VI. THE QUASIELASTIC REACTION CHANNELS

Table VII is a summary of the cross sections for different channels, at the incident energies where measurements of the transfer reactions were performed, in addition to fusion and elastic scattering which are known in a wider energy range. In Ref. 14, the various transfer channels were identified and their Q-value integrated cross sections were individually obtained, but here the column named $\sigma_{\rm tr}$ lists the total transfer cross sections. We performed recently further measurements with the ^{32}S beam so that the reported transfer cross sections differ slightly from the previous work[14] in some cases. Also, the $\sigma_{\rm tr}$ for 92.8 MeV $^{32}{\rm S}+^{58}{\rm Ni}$ and 90.3 and 81.8 MeV $^{32}{\rm S}+^{64}{\rm Ni}$ were not published before.

The inelastic cross sections $\sigma_{\rm in}$ are not experimental values, as these are not available. They result from the same coupled-channels calculations described in Sec. V, which are usually quite reliable for inelastic excitations. In fact, the results are not so different from the calculations of Ref. 14, where a standard potential was used.

By summing $\sigma_{\rm tr}$, $\sigma_{\rm in}$, and $\sigma_{\rm fus}$ we obtain the quasiexperimental cross sections named $\sigma_{\rm sum}$ which can be compared with the total reaction cross sections σ_r deduced from the elastic scattering fits. The comparison, taking into account the uncertainties in the ingredients of $\sigma_{\rm sum}$, indicates a substantial agreement between the two sets of numbers, with some tendency for $\sigma_{\rm sum}$ to overestimate σ_r for $^{32}{\rm S}+{\rm Ni}$ except for the lowest energies.

Interesting trends are observed in the $\sigma_{\rm tr}$ and σ_{in} values, which clearly appear in Fig. 13 where those cross sections have been plotted versus the energy distance from the barrier.[15] The four systems are divided in two pairs, $^{32}{\rm S}+^{64}{\rm Ni}$ and $^{36}{\rm S}+^{58}{\rm Ni}$, having transfer cross sections larger than the other two cases by factors 3–5, depending on the energy. An analogous situation shows up for the (calculated) inelastic cross sections, where now the $^{32}{\rm S}+{\rm Ni}$ systems are somewhat favored with respect to the other two. $^{32}{\rm S}+^{64}{\rm Ni}$ is therefore "unique," having larger transfer cross sections and/or stronger inelastic excitations than any other system. This is why its imaginary potential at $r_{1/4}$ is so large and a correlation with its larger sub-barrier fusion enhancement and threshold anomaly is also established.

VII. CONCLUSIONS

Elastic scattering measurements were performed in the four systems $^{32,36}{\rm S}+^{58,64}{\rm Ni}$ at various energies close to the barrier, providing us with detailed and systematic information, which supplements what was already known on the competing reaction channels such as quasielastic transfer and fusion. The scattering data were analyzed within the optical model and good fits were obtained in most cases, by separating the absorption in a surface part (simulating the quasielastic reaction channels) and in a more internal fusion potential. However, it seems that choosing such volume absorption to be confined inside the barrier forces the surface potential to be quite strong (and sharp) in many cases, so that the total imaginary potential has unusual shapes with an evident secondary pocket. The conclusion is that an analysis as in Refs. 11 and 17, where the fusion potential has a larger range, is probably more appropriate. An interesting systematic trend of the surface potential radius has been observed anyway, scaling with the number of neutrons and neutron holes away from closed shells in the colliding nuclei.

The threshold anomaly of the potentials shows up in all cases, being more conspicuous in $^{32}{\rm S}+^{64}{\rm Ni}$ where the sub-barrier fusion has the largest enhancement as well. The fitting potentials satisfy qualitatively the dispersion relation.

Coupled-channels calculations of elastic scattering and fusion were performed, considering the lowest collective inelastic excitations of projectile and target. The scattering cross sections are overpredicted in all cases and the fusion cross sections are satisfactorily calculated only in the case of $^{32}{\rm S}+^{58}{\rm Ni}$, being otherwise lower than the experiment. The discrepancy is largest for $^{32}{\rm S}+^{64}{\rm Ni}$. All this shows the (isotopic dependent) importance of including the quasielastic transfer in a coupled-channels description of both elastic scattering and fusion. No attempt has been made here to explicitly couple such transfer channels, also in view of the fact that simplified CC calculations including transfer had already been performed for the same systems in previous papers.[13,14] Further analyses in that sense would be useful, on condition that a more rigorous treatment of the transfer channels is done.

Fusion excitation functions were also calculated in the energy-dependent barrier penetration model using the real part of the fitting potentials to produce the Coulomb barrier at each energy. The resulting cross sections are systematically larger than the CC calculations and also overestimate somewhat the experimental values, but the overall agreement is fair in all cases.

The comparison between total cross sections and fusion plus quasielastic cross sections shows a good overall agreement. $^{32}S+^{64}Ni$ have comparable total transfer cross sections, larger than in the other two systems. In addition, the coupled-channels calculations of the inelastic excitations predict larger cross sections for the two $^{32}S+Ni$ systems.

In summary, (i) we have indications that the size of the fusion potential should be larger than assumed in Ref. 10; (ii) we have demonstrated the need for including explicitly transfer channels in a coupled-channels scheme, in order to fully understand the low energy S+Ni collisions; when considering the fusion, $^{32}S+^{64}Ni$ shows the most clear-cut evidence of this; (iii) sub-barrier fusion enhancement, quasielastic cross section, threshold anomaly, and imaginary potential near the strong absorption radius are intercorrelated; (iv) the energy-dependent fitting potentials give fairly good predictions for the sub-barrier fusion. However, the ambiguities inherent in extracting fusion cross sections from those potentials are large, and the need for experimental information on spin distributions is strongly felt.

ACKNOWLEDGMENTS

We are pleased to acknowledge valuable discussions with R. A. Broglia, C. H. Dasso, S. Landowne, M. A. Nagarajan, and T. Udagawa. The precious assistance of the Tandem staff at Laboratori Nazionali di Legnaro during the experiments is gratefully acknowledged. We also thank Y. Nagashima and G. Fortuna, who joined part of the experiments.

---

*On leave from CNEA, Laboratorio TANDAR, Buenos Aires, Argentina.

[1] *Proceedings of the International Symposium on Heavy Ion Interactions Around the Coulomb Barrier, Legnaro (Italy), 1988*, Vol. 317 of *Lecture Notes in Physics*, edited by C. Signorini, S. Skorka, P. Spolaore, and A. Vitturi (Springer, Berlin, 1988).

[2] M. Beckerman, Rep. Prog. Phys. **51**, 1047 (1988).

[3] C. H. Dasso, S. Landowne, and A. Winther, Nucl. Phys. **A405**, 381 (1983); R. A. Broglia, C. H. Dasso, S. Landowne, and G. Pollarolo, Phys. Lett. **133B**, 34 (1983); M. J. Rhoades-Brown and P. Braun-Munzinger, *ibid.* **136B**, 19 (1984); S. C. Pieper, M. J. Rhoades-Brown, and S. Landowne, *ibid.* **162B**, 43 (1985).

[4] J. S. Lilley, B. R. Fulton, M. A. Nagarajan, I. J. Thompson, and D. W. Banes, Phys. Lett. **151B**, 181 (1985).

[5] A. Baeza, B. Bilwes, R. Bilwes, J. Diaz, and J. L. Ferrero, Nucl. Phys. **A419**, 412 (1984); B. Bilwes, R. Bilwes, L. Stuttgé, F. Ballester, J. Diaz, J. L. Ferrero, C. Roldan, and F. Sanchez, *ibid.* **473**, 353 (1987).

[6] M. A. Nagarajan, C. Mahaux, and G. R. Satchler, Phys. Rev. Lett. **54**, 1136 (1985); C. Mahaux, H. Ngo, and G. R. Satchler, Nucl. Phys. **A449**, 354 (1986).

[7] B. R. Fulton, D. W. Banes, J. S. Lilley, M. A. Nagarajan, and I. J. Thompson, Phys. Lett. **162B**, 55 (1985).

[8] A. M. Stefanini, D. Bonamini, A. Tivelli, G. Montagnoli, G. Fortuna, Y. Nagashima, S. Beghini, C. Signorini, A. DeRosa, G. Inglima, M. Sandoli, G. Cardella, and F. Rizzo, Phys. Rev. Lett. **59**, 2852 (1987).

[9] H. Delagrange, L. C. Vaz, and J. M. Alexander, Phys. Rev. C **20**, 1731 (1979).

[10] G. R. Satchler, M. A. Nagarajan, J. S. Lilley, and I. J. Thompson, Ann. Phys. (N.Y.) **178**, 110 (1987).

[11] S. W. Hong, T. Udagawa, and T. Tamura, Nucl. Phys. **A491**, 492 (1989).

[12] P. H. Stelson, Phys. Lett. B **205**, 190 (1988).

[13] A. M. Stefanini, G. Fortuna, R. Pengo, W. Meczynski, G. Montagnoli, L. Corradi, A. Tivelli, S. Beghini, C. Signorini, S. Lunardi, M. Morando, and F. Soramel, Nucl. Phys. **A456**, 509 (1986).

[14] A. M. Stefanini, G. Montagnoli, G. Fortuna, R. Menegazzo, S. Beghini, C. Signorini, A. DeRosa, G. Inglima, M. Sandoli, F. Rizzo, G. Pappalardo, and G. Cardella, Phys. Lett. B **185**, 15 (1987).

[15] L. C. Vaz, J. M. Alexander, and G. R. Satchler, Phys. Rep. **69**, 373 (1981).

[16] M. H. Macfarlane and S. C. Pieper, Argonne National Laboratory Report ANL-76-11 (Rev. 1), 1978; M. Rhoades-Brown, M. H. Macfarlane, and S. C. Pieper, Phys. Rev. C **21**, 2417 (1980).

[17] T. Udagawa, in *Proceedings of the International Symposium on Heavy Ion Interactions Around the Coulomb Barrier, Legnaro (Italy), 1988* (Ref. 1), p. 191.

[18] G. R. Satchler, private communication.

[19] M. A. Nagarajan and G. R. Satchler, Phys. Lett. B **173**, 29 (1986).

[20] C. H. Dasso, S. Landowne, and G. Pollarolo, Phys. Lett. B **217**, 25 (1989).